NASA Technical Paper 3548

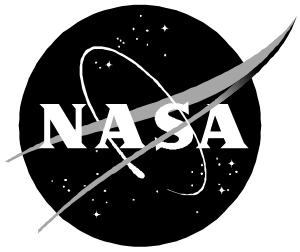

Analysis of Three-Dimensional-Cavity-Backed Aperture Antennas Using a Combined Finite Element Method / Method of Moments / Geometrical Theory of Diffraction Technique

C. J. Reddy
Langley Research Center • Hampton, Virginia

M. D. Deshpande
ViGYAN, Inc. • Hampton, Virginia

C. R. Cockrell and F. B. Beck
Langley Research Center • Hampton, Virginia

National Aeronautics and Space Administration
Langley Research Center • Hampton, Virginia 23681-0001

November 1995

Acknowledgments

The authors would like to thank Carl A. Lipp, Robert Holt, and Hunter Walden for fabricating the coaxial cavity and performing the experiments.

Available electronically at the following URL address: http://techreports.larc.nasa.gov/ltrs/ltrs.html

Printed copies available from the following:

NASA Center for AeroSpace Information
800 Elkridge Landing Road
Linthicum Heights, MD 21090-2934
(301) 621-0390

National Technical Information Service (NTIS)
5285 Port Royal Road
Springfield, VA 22161-2171
(703) 487-4650

Abstract

A combined finite element method (FEM) and method of moments (MoM) technique is presented to analyze the radiation characteristics of a cavity-fed aperture in three dimensions. Generalized feed modeling has been done using the modal expansion of fields in the feed structure. Numerical results for some feeding structures such as a rectangular waveguide, circular waveguide, and coaxial line are presented. The method also uses the geometrical theory of diffraction (GTD) to predict the effect of a finite ground plane on radiation characteristics. Input admittance calculations for open radiating structures such as a rectangular waveguide, a circular waveguide, and a coaxial line are presented. Numerical data for a coaxial-fed cavity with finite ground plane are verified with experimental data.

1. Introduction

Cavity-backed aperture antennas are very popular in aerospace applications because of their conformal nature. The cavities can also have various types of microstrip antennas residing in them. Hybrid techniques have recently become attractive for the numerical analysis of these types of problems. The combined finite element method and method of moments (FEM and MoM) techniques, in particular, have been used to analyze various cavity-backed antenna systems (ref. 1).

The FEM has a relatively simple formulation and is attractive for complex penetrable structures. Also, it results in sparse, banded matrices that can be effectively stored and solved. However, the FEM when used alone does not incorporate the Sommerfield radiation condition and hence requires discretization to extend far from the source region so that the radiation condition can be imposed. Recent efforts have concentrated on the use of absorbing boundary conditions to reduce the discretization region (ref. 2). Unfortunately, the accuracy of these approximate boundary conditions depends on specific problem geometry, leading to results of unpredictable accuracy.

The method of moments (MoM), on the other hand, incorporates the Sommerfield radiation condition through the use of the appropriate Green's function. As a result, the domain discretization can be kept to a minimum. However, this method has the disadvantage of being difficult to implement for complex penetrable structures. This method also results in full matrices whose treatment requires excessive storage, limiting its application to small-scale devices.

To eliminate the disadvantages of both methods, several authors have proposed a combined approach (refs. 3 and 4) for radiation and scattering problems. For a comprehensive list of references on hybrid FEM/MoM techniques, see reference 5, chapter 9.

The modeling of the coaxial feed in reference 1 is accomplished by replacing the feed probe by a constant filament of current with a delta-gap generator. The feed modeling in reference 1 is expected to give good results for shallow cavities, but deep cavities require rigorous feed modeling. In this paper a combined FEM/MoM approach is used to predict characteristics of cavity-backed antennas (fig. 1). Various feed lines such as a rectangular waveguide, a circular waveguide, and a coaxial line are considered. Using the modal expansions of fields in the feed, the input admittance of cavity-backed antennas is calculated accurately.

In most antenna-pattern measurements, the infinite ground plane is simulated by a relatively large finite ground plane. Although this simulation does not appreciably affect the input admittance measurements, diffractions from the edges of the ground plane modify the radiation pattern considerably. In the past, the geometrical theory of diffraction (GTD) was successfully applied to predict the changes in the radiation pattern of the aperture antennas caused by a finite ground plane (ref. 6). The technique

described in reference 6 predicts the changes in the radiation patterns of cavity-backed aperture antennas with finite ground planes.

The body of this paper is organized in the following manner. Section 2 presents the theory for cavity-backed apertures in infinite ground planes. Section 3 compares the numerical results calculated using the present analysis with the available results in the literature. The input admittance calculations for an open rectangular waveguide, a circular waveguide, and a coaxial line are presented and compared with the results available in the literature. To verify the validity of the GTD technique used in combination with the FEM/MoM technique, the radiation patterns of a coaxial cavity with finite ground plane are calculated and compared with experimental results measured at the Langley Low-Frequency Antenna Test Facility. Numerical data for input return loss of such a coaxial cavity are also computed and compared with experimental data. Section 4 presents concluding remarks. For completeness, an appendix includes expressions for modal expansions of electric fields of input-feed-line structures.

Symbols

$\mathbf{A}$	FEM/MoM matrix
A_{pq}, B_{pq}	amplitude of modal vectors in feed
a, b	length and width of rectangular waveguide, respectively
a_m	reflection coefficients for TEM/TE modes
$\mathbf{b}$	excitation matrix
b_m	reflection coefficients for TM modes
D_s, D_h	diffraction coefficients
ds	surface integral
dv	volume integral
$\mathbf{E}$	time-harmonic electric field
$\mathbf{E}_{\text{inc}}$	incident electric field
$\mathbf{E}_{\text{inp}}$	electric field coming from transmission line input
$\mathbf{e}$	unknown coefficient matrix
e_i	unknown coefficients as defined in equation (8)
$\mathbf{e}_{\text{inc}}$	modal vector function for incident electric field in feed structure
$\mathbf{e}_m^{TE}$	TEM/TE modes in feed line
$\mathbf{e}_m^{TM}$	TM modes in feed line
$\mathbf{F}$	electric vector potential
$\mathbf{H}$	time-harmonic magnetic field
$\mathbf{H}_{ap}$	magnetic field at aperture
$\mathbf{H}^d$	total diffracted magnetic field
$\mathbf{H}_A^d$	diffracted magnetic field from point A
$\mathbf{H}_B^d$	diffracted magnetic field from point B
$\mathbf{H}_C^d$	diffracted magnetic field from point C

$\mathbf{H}_D^d$	diffracted magnetic field from point D
$\mathbf{H}_{ff}$	far field of magnetic field
$\mathbf{H}_{ff}^t$	total magnetic far field after adding diffracted field
$\mathbf{H}_{\text{inp}}$	magnetic field at input surface
$H_{\theta ff}$	magnetic far field, θ-component
$H_{\phi ff}$	magnetic far field, ϕ-component
$H_{\theta,\,A}^d$	diffracted magnetic field from point A, θ-component
$H_{\phi,\,A}^d$	diffracted magnetic field from point A, ϕ-component
$H_{\theta,\,B}^d$	diffracted magnetic field from point B, θ-component
$H_{\phi,\,B}^d$	diffracted magnetic field from point B, ϕ-component
$J_1(\,)$	Bessel function of first kind (first order)
$J_n(\,)$	Bessel function of first kind (nth order)
$J_n'(\,)$	derivative of $J_n(\,)$ with respect to its argument
j	$= \sqrt{-1}$
k_o	free-space wave number, $\frac{2\pi}{\lambda}$
k_ρ	cutoff wave number for TM modes in circular waveguide
k_ρ'	cutoff wave number for TE modes in circular waveguide
L	distance between radiating aperture (in $z = 0$ plane) and feed-line input surface (in $z = -L$ plane)
L_i	length of edge of tetrahedral element
$\mathbf{M}$	magnetic current
n	wedge factor
$\hat{n}$	unit normal
p, q	mode indices for feed
$\mathbf{r}$	position vector from origin to field point
$\mathbf{r}'$	position vector from origin to source point
r_c	radius of circular waveguide
r_1, r_2	inner and outer radius of coaxial line, respectively
r, θ, ϕ	spherical coordinates
S	surface area
S_{ap}	surface area of aperture (fig. 1)
S_{inp}	surface area of input plane (fig. 1)
$\mathbf{T}$	vector testing function for volume elements
$\mathbf{T}_s$	vector testing function for surface elements

TE	transverse electric
TE_{10}	dominant mode in rectangular waveguide
TE_{11}	dominant mode in circular waveguide
TEM	transverse electric and magnetic
TM	transverse magnetic
V	volume
$\mathbf{W}_i$	vector basis functions for tetrahedral elements, i = 1, 2, …, 6
$\mathbf{W}_j$	vector basis functions for tetrahedral elements, j = 1, 2, …, 6
W_1, W_2	length and width of finite ground plane, respectively (fig. 1)
X, Y, Z	rectangular coordinate axes (fig. 1)
x, **y**, **z**	unit vector along X-, Y-, and Z-axis, respectively (fig. 1)
Y_{in}	input admittance of feed line
Y_o	characteristic admittance of feed transmission line
α_m, α_n	simplex coordinates associated with nodes m and n in tetrahedral element
β_o'	angle between edge of diffraction and ray of incidence on edge
Γ	reflection coefficient as defined in equation (27)
γ_{inc}	propagation constant of incident field in feed
γ_m	propagation constant of feed line
ε_{op}, ε_{oq}	Neumann's number
ε_r	relative permittivity
η_o	intrinsic impedance of free space
$\hat{\theta}$	unit vector along θ-direction
λ	free-space wavelength
μ_o	free-space permeability
μ_r	relative permeability
ξ_1	angle between ground plane and diffracted ray from point A
ξ_2	angle between ground plane and diffracted ray from point B
ρ_{cA}	distance between center of aperture and diffraction point A
ρ_{cB}	distance between center of aperture and diffraction point B
ρ_{cC}	distance between center of aperture and diffraction point C
ρ_{cD}	distance between center of aperture and diffraction point D
ρ, ϕ, z	cylindrical coordinates
$\hat{\rho}$, $\hat{\phi}$, $\hat{z}$	unit vector along ρ-, ϕ-, and z-direction, respectively
$\hat{\phi}$	unit vector along ϕ-direction
χ_{pq}	pth zero (p = 1, 2, 3…) of J_n ( )

χ'_{pq} pth zero (p = 1, 2, 3…) of ( )

ψ_o angle between aperture (source) and point of diffraction

ω angular frequency

▲ integration over a tetrahedral element

∇ del operator

2. Theory

Figure 1 shows the geometry of the problem to be analyzed. For a linear, isotropic, and source-free region the electric field satisfies the vector wave equation:

$$\nabla \times \left(\frac{1}{\mu_r} \nabla \times \mathbf{E} \right) - k_o^2 \varepsilon_r \mathbf{E} = 0 \tag{1}$$

where μ_r and ε_r are the relative permeability and relative permittivity of the medium in the cavity. The current formulation can be easily modified to incorporate anisotropic materials by using proper tensor quantities for μ_r and ε_r (ref. 7). The time variation exp ($j\omega t$) is assumed and suppressed throughout this paper.

To facilitate the suitable solution of the partial differential equation in equation (1) with the FEM, equation (1) is multiplied by a vector testing function **T,** and the result is integrated over the volume of the cavity. By applying suitable vector identities, we can write equation (1) in its weak form (ref. 8) as

$$\iiint_V \frac{1}{\mu_r} (\nabla \times \mathbf{T}) \cdot (\nabla \times \mathbf{E}) dv - k_o^2 \varepsilon_r \iiint_V \mathbf{T} \cdot \mathbf{E} dv = \iiint_V \nabla \cdot \left(\mathbf{T} \times \frac{1}{\mu_r} \nabla \times \mathbf{E} \right) dv \tag{2}$$

Applying the divergence theorem to the integral on the right-hand side of equation (2) and using Maxwell's equation $\nabla \times \mathbf{E} = -j\omega\mu_o\mu_r\mathbf{H}$, where μ_o is the permeability of free space and ω is the angular frequency, we can write equation (2) as

$$\iiint_V \frac{1}{\mu_r} (\nabla \times \mathbf{T}) \cdot (\nabla \times \mathbf{E}) dv - k_o^2 \varepsilon_r \iiint_V \mathbf{T} \cdot \mathbf{E} dv = j\omega\mu_o \iint_S (\mathbf{T} \times \hat{n}) \cdot \mathbf{H} ds \tag{3}$$

where $\hat{n}$ is the outward unit normal to the surface and **H** is the magnetic field at the surface. Because the tangential electric field is zero on the perfect-electric-conducting (PEC) walls of the cavity, the surface integral in equation (3) is nonzero only over the aperture opening in the infinite ground plane and the input aperture. Hence, we can write equation (3) as

$$\iiint_V \frac{1}{\mu_r} (\nabla \times \mathbf{T}) \cdot (\nabla \times \mathbf{E}) dv - k_o^2 \varepsilon_r \iiint_V \mathbf{T} \cdot \mathbf{E} dv - j\omega\mu_o \iint_{S_{ap}} (\mathbf{T} \times \hat{n}) \cdot \mathbf{H}_{ap} ds = j\omega\mu_o \iint_{S_{\text{inp}}} (\mathbf{T} \times \hat{n}) \cdot \mathbf{H}_{\text{inp}} ds \tag{4}$$

where S_{ap} is the aperture surface and S_{inp} is the input surface (see fig. 1), $\mathbf{H}_{ap}$ is the magnetic field at the aperture, and $\mathbf{H}_{\text{inp}}$ is the magnetic field at the input surface.

At this point, the problem can be divided into three parts, the first part involving the discretization and evaluation of volume integrals on the left-hand side of equation (4) and the second part involving

the discretization and evaluation of the surface integral over S_{ap}. The third part involves the surface integral over the input aperture. These three parts are given explicitly as

$$I_v = \iiint_V \frac{1}{\mu_r}(\nabla \times \mathbf{T}) \cdot (\nabla \times \mathbf{E}) dv - k_o^2 \varepsilon_r \iiint_V \mathbf{T} \cdot \mathbf{E} dv \tag{5}$$

$$I_{ap} = -j\omega\mu_o \iint_{S_{ap}} (\mathbf{T} \times \hat{n}) \cdot \mathbf{H}_{ap} ds \tag{6}$$

$$I_{\text{inp}} = j\omega\mu_o \iint_{S_{\text{inp}}} (\mathbf{T} \times \hat{n}) \cdot \mathbf{H}_{\text{inp}} ds \tag{7}$$

2.1. FEM Formulation

To discretize the volume integrals in equation (5), the volume of the cavity is subdivided into small-volume tetrahedral elements. The electric field is expressed in terms of the edge vector basis functions (ref. 5), which enforce the divergenceless condition of the electric field implicitly:

$$\mathbf{E} = \sum_{i=1}^{6} e_i \mathbf{W}_i \tag{8}$$

where e_i are the unknown coefficients associated with each edge of the tetrahedral element and

$$\mathbf{W}_i = L_i(\alpha_m \nabla \alpha_n - \alpha_n \nabla \alpha_m) \tag{9}$$

where m and n are the nodes connected to form edge i, L_i is the length of the ith edge, and α_m and α_n are the simplex coordinates associated with nodes m and n (ref. 8).

The testing function **T** is taken to be the same set of basis functions as that given in equation (8); that is,

$$\mathbf{T} = \mathbf{W}_j \qquad (j = 1, 2, \ldots, 6) \tag{10}$$

Substituting equations (8) and (10) into equation (5) and integrating over the volume of each element yields

$$I_{ev} = \frac{1}{\mu_r} \sum_{i=1}^{6} \iiint_{\blacktriangle} (\nabla \times \mathbf{W}_i) \cdot (\nabla \times \mathbf{W}_j) e_i dv - k_o^2 \varepsilon_r \iiint_{\blacktriangle} (\mathbf{W}_i \cdot \mathbf{W}_j) e_i dv \qquad (j = 1, 2, \ldots, 6) \tag{11}$$

where ▲ indicates the integration over the volume of a tetrahedral element and I_{ev} represents the integral I_v over a single element volume.

The evaluation of these integrals over a tetrahedral element is given in reference 9. These element matrices are assembled over all the elements in the cavity volume to form a symmetric, sparse matrix of FEM.

2.2. MoM Formulation

The discretization of cavity volume into tetrahedral elements automatically results in the discretization of the aperture into triangular elements at the $z = 0$ plane. In accordance with the equivalence principle (ref. 10), the fields in the two regions can be decoupled by closing the aperture with a perfect electric conductor and introducing the equivalent magnetic current

$$\mathbf{M} = \mathbf{E} \times \mathbf{z} \qquad (z = 0) \tag{12}$$

over the extent of the aperture. Hence, from equation (8), the magnetic current over a triangular element can be expressed in terms of the unknown coefficients associated with the tetrahedral elements as

$$\mathbf{M} = \sum_{i=1}^{3} e_i(\mathbf{W}_i \times \mathbf{z})\Big|_{z=0} \tag{13}$$

Similarly the testing functions can be modified as

$$\mathbf{T}_s = \mathbf{T} \times \mathbf{z} = \mathbf{W}_j \times \mathbf{z} \qquad (j = 1, 2, 3) \tag{14}$$

The magnetic field caused by the magnetic current given in equation (13) above the infinite ground plane is given by

$$\mathbf{H}_{ap} = \frac{1}{j\omega\mu_o}(\nabla \times \nabla \times \mathbf{F}) \tag{15}$$

where the electric vector potential **F** (making use of the image theory) is given by

$$\mathbf{F} = \frac{1}{2\pi}\iint_{S_{ap}} \mathbf{M}(x', y')\frac{\exp(-jk_o|\mathbf{r}-\mathbf{r}'|)}{|\mathbf{r}-\mathbf{r}'|}dx'dy' \tag{16}$$

where **r** is the field point and **r′** is the source point.

Using the appropriate vector identities, we can rewrite the equation for the radiated magnetic field in equation (15) as (ref. 10)

$$\mathbf{H}_{ap} = \frac{1}{j\omega\mu_o}[k_o^2\mathbf{F} + \nabla(\nabla \cdot \mathbf{F})] \tag{17}$$

Substituting equation (17) into equation (6) and using standard surface vector calculus formulas (ref. 11) yields

$$I_{ap} = -k_o^2\iint_{S_{ap}} \mathbf{T}_s \cdot \mathbf{F}ds + \iint_{S_{ap}} (\nabla \cdot \mathbf{T}_s)(\nabla \cdot \mathbf{F})ds \tag{18}$$

The integrals in the above equation are evaluated over all the triangles on the aperture surface following the procedure outlined in Rao et al. (ref. 11). When calculating the mutual term over the triangles, a 13-point Gaussian quadrature formula developed for triangles (ref. 12) is used. Closed-form expressions given by Wilton et al. (ref. 13) are used to evaluate the self term of these integrals. The dense matrix thus formed is assembled over all the triangles and combined with the FEM matrix using a global numbering system.

2.3. Input Integral

For any transmission line input, the electric field can be formulated as the sum of the incident and reflected fields.

$$\mathbf{E}_{\text{inp}} = \mathbf{E}_{\text{inc}} + \sum_m [a_m\mathbf{e}_m^{TE}(x, y) + b_m\mathbf{e}_m^{TM}(x, y)]\exp(\gamma_m z) \tag{19}$$

$$\mathbf{E}_{\text{inc}} = \mathbf{e}_{\text{inc}}\exp(-\gamma_{\text{inc}}z) \tag{20}$$

where $\mathbf{E}_{\text{inc}}$ is the incident electric field with unit amplitude, $\mathbf{e}_m^{TE}$ and $\mathbf{e}_m^{TM}$ represent the TEM/TE[1] and the TM mode, respectively, a_m and b_m are the reflection coefficients for the TEM/TE and the TM mode, respectively, and γ_m is the propagation constant. With the orthogonality properties of the waveguide modes (ref. 10), the reflection coefficients are

$$a_m = \exp(-\gamma_m z)\iint_{S_{\text{inp}}} \mathbf{e}_m^{TE} \cdot (\mathbf{E} - \mathbf{E}_{\text{inc}})\,dx\,dy \tag{21}$$

$$b_m = \exp(-\gamma_m z)\iint_{S_{\text{inp}}} \mathbf{e}_m^{TM} \cdot (\mathbf{E} - \mathbf{E}_{\text{inc}})\,dx\,dy \tag{22}$$

The magnetic field at the waveguide input is given by

$$\mathbf{H}_{\text{inp}} = -\frac{1}{j\omega\mu_o}\left(\frac{1}{\mu_r}\nabla \times \mathbf{E}_{\text{inp}}\right) \tag{23}$$

Substituting a_m and b_m in equation (23) and then using equation (23) in equation (7) and integrating over the feed-line cross section at $z = -L$, we can write equation (7) as

$$\begin{aligned} I_{\text{inp}} = {} & 2\gamma_{\text{inc}}\exp(\gamma_{\text{inc}}L)\iint_{S_{\text{inp}}} \mathbf{T} \cdot \mathbf{e}_{\text{inc}}\,dx\,dy \\ & - \sum_m \gamma_m \left(\iint_{S_{\text{inp}}} \mathbf{T} \cdot \mathbf{e}_m^{TE}\,dx\,dy\right)\left(\iint_{S_{\text{inp}}} \mathbf{E} \cdot \mathbf{e}_m^{TE}\,dx\,dy\right) \\ & + \sum_m \frac{k_o^2}{\gamma_m}\left(\iint_{S_{\text{inp}}} \mathbf{T} \cdot \mathbf{e}_m^{TM}\,dx\,dy\right)\left(\iint_{S_{\text{inp}}} \mathbf{E} \cdot \mathbf{e}_m^{TM}\,dx\,dy\right) \end{aligned} \tag{24}$$

2.4. FEM/MoM Matrix Equation

Combining all the integrals given in equations (5)–(7), we can write the system equation for this problem as

$$\begin{aligned} & \iiint_V \frac{1}{\mu_r}(\nabla \times \mathbf{T}) \cdot (\nabla \times \mathbf{E})\,dv - k_o^2\varepsilon_r \iiint_V \mathbf{T} \cdot \mathbf{E}\,dv - j\omega\mu_o \iint_{S_{ap}} (\mathbf{T} \times \hat{n}) \cdot \mathbf{H}_{ap}\,ds \\ & \quad + \sum_m \gamma_m \left(\iint_{S_{\text{inp}}} \mathbf{T} \cdot \mathbf{e}_m^{TE}\,dx\,dy\right)\left(\iint_{S_{\text{inp}}} \mathbf{E} \cdot \mathbf{e}_m^{TE}\,dx\,dy\right) \\ & \quad - \sum_m \frac{k_o^2}{\gamma_m}\left(\iint_{S_{\text{inp}}} \mathbf{T} \cdot \mathbf{e}_m^{TM}\,dx\,dy\right)\left(\iint_{S_{\text{inp}}} \mathbf{E} \cdot \mathbf{e}_m^{TM}\,dx\,dy\right) \\ & \quad = 2\gamma_{\text{inc}}\exp(\gamma_{\text{inc}}L)\iint_{S_{\text{inp}}} \mathbf{T} \cdot \mathbf{e}_{\text{inc}}\,dx\,dy \end{aligned} \tag{25}$$

[1]Because the analysis is assumed to be valid for a generalized feed line, both TEM and TE modes are represented. They need only be used when applicable.

Substituting the expansion functions for **E** and **T** converts this equation into a set of linear equations to solve for the unknown e_i given in equation (8). The linear equation system to be solved is written in matrix form as

$$\mathbf{Ae} = \mathbf{b} \tag{26}$$

where **A** is a partly sparse (from the FEM) and partly dense (from the MoM and the modal expansion method) matrix, **b** is the excitation vector, and **e** is the unknown vector to be solved. The biconjugate gradient algorithm is used with diagonal preconditioning (ref. 14) to solve equation (26) efficiently. This algorithm also makes use of the symmetry of the matrix to store the matrix effectively.

2.5. Reflection Coefficient and Input Admittance

Solving equation (25) and using equations (21) and (22), we can obtain the reflection coefficients of any waveguide mode:

$$\Gamma = a_m \text{ or } \Gamma = b_m \tag{27}$$

The input admittance is then calculated as

$$Y_{in} = \frac{1-\Gamma}{1+\Gamma} Y_o \tag{28}$$

where Y_o is the characteristic admittance of the feed transmission line.

2.6. Far Field With Infinite Ground Plane

Once the electric field in the aperture is known, using equation (13) for the magnetic current, the magnetic far field with infinite ground plane can be evaluated directly from the following equation:

$$\mathbf{H}_{ff}(r, \theta, \phi)\big|_{r\to\infty} = -\frac{jk_o}{\eta_o}\frac{\exp(-jk_o r)}{2\pi r}\iint_{S_{ap}} (\hat{\theta}\hat{\theta} + \hat{\phi}\hat{\phi}) \cdot \mathbf{M}(x, y)\exp[jk_o \sin\theta(x\cos\phi + y\sin\phi)]\,dx\,dy \tag{29}$$

2.7. Application of GTD for Finite Ground Planes

The infinite-ground-plane solution described in the preceding sections yields the field radiated in the forward direction. This solution is obtained with equation (29). The effect of the finite ground plane is incorporated by using the compact edge diffraction coefficients (ref. 15) and following the procedure described in reference 6. The radiation fields are supplemented by the additional field contributions arising from the diffraction by the edges of the finite ground plane. The diffracted field supplements the field in the forward region, whereas it accounts totally for the field in the shadow region (behind the finite ground plane) where the infinite-ground-plane solution gives a zero field.

The geometry of the finite rectangular ground plane is illustrated in figure 1. The midpoints on the two edges of length W_2 are given by *A* and *B*, respectively. The midpoints on the two edges of length W_1 are given by *C* and *D*, respectively. The diffracted fields from *A* and *B* are given by (ref. 6)

$$H^d_{\theta,A} \approx \frac{1}{2} H_{\theta ff}\left(d, \frac{\pi}{2}, 0\right) D_s(\rho_{cA}, \xi_1, \psi_o, \beta'_o, n)\left[\frac{\rho_{cA}}{r(r+\rho_{cA})}\right]^{1/2} \exp(-jk_o r)\exp(jk_o d\sin\theta) \tag{30}$$

$$H^d_{\theta,B} \approx \frac{1}{2} H_{\theta ff}\left(d, \frac{\pi}{2}, \pi\right) D_s(\rho_{cB}, \xi_2, \psi_o, \beta'_o, n)\left[\frac{\rho_{cB}}{r(r+\rho_{cA})}\right]^{1/2} \exp(-jk_o r)\exp(-jk_o d\sin\theta) \tag{31}$$

for ϕ polarization, and

$$H^d_{\phi,\,A} \approx \frac{1}{2} H_{\phi ff}\left(d, \frac{\pi}{2}, 0\right) D_h(\rho_{cA}, \xi_1, \psi_o, \beta'_o, n)\left[\frac{\rho_{cA}}{r(r+\rho_{cA})}\right]^{1/2} \exp(-jk_o r)\exp(jk_o d\sin\theta) \tag{32}$$

$$H^d_{\phi,\,B} \approx \frac{1}{2} H_{\phi ff}\left(d, \frac{\pi}{2}, \pi\right) D_h(\rho_{cB}, \xi_2, \psi_o, \beta'_o, n)\left[\frac{\rho_{cB}}{r(r+\rho_{cA})}\right]^{1/2} \exp(-jk_o r)\exp(-jk_o d\sin\theta) \tag{33}$$

for θ polarization. In the preceding equations,

$$\rho_{cA} = \rho_{cB} = d = \frac{W_1}{2} \tag{34}$$

and

$$\xi_1 = \frac{\pi}{2} + \theta \quad \text{for} \quad 0 \le \theta \le \pi \tag{35}$$

$$\xi_2 = \begin{cases} \dfrac{\pi}{2} - \theta & \text{for } 0 \le \theta \le \dfrac{\pi}{2} \\ \dfrac{5\pi}{2} - \theta & \text{for } \dfrac{\pi}{2} < \theta \le \pi \end{cases} \tag{36}$$

where

ψ_o angle of incidence from aperture (source) toward the point of diffraction (*A* or *B*) = 0°

β'_o $\frac{\pi}{2}$ for normal incidence (ref. 15, p. 811)

n wedge factor (ref. 15, figs. 13–30)

Similarly, the diffracted fields from *C* and *D* are also calculated by replacing $\rho_{cC} = \rho_{cD} = d = W_2/2$. The detailed expressions for diffraction coefficients D_s and D_h are given by equation (113) of reference 15. Total diffracted field is given by

$$\mathbf{H}^d = \begin{cases} \mathbf{H}^d_A + \mathbf{H}^d_B & \text{for } \phi = 0° \text{ plane} \\ \mathbf{H}^d_C + \mathbf{H}^d_D & \text{for } \phi = 90° \text{ plane} \end{cases} \tag{37}$$

The diffracted fields for the $\phi = 180°$ and $\phi = 270°$ planes can also be calculated in a similar manner. The total radiated far field is given by adding the diffracted field and magnetic far field given in equation (29); that is,

$$\mathbf{H}^t_{ff} = \mathbf{H}_{ff} + \mathbf{H}^d \tag{38}$$

The preceding analysis can be easily extended to a circular finite ground plane. If the circular ground plane is symmetrically excited, the diffracted rays come to a focus in the forward and the rear axial direction; that is, the axis of symmetry is a caustic of diffracted rays. The GTD field is not valid at the caustic. However, GTD can be used indirectly to calculate the equivalent edge currents (around the rim of the ground plane) that radiate in the caustic direction; these edge currents are integrated around the circular rim to yield the field in the neighborhood of the caustic. The radiated field evaluation is the same as that described in reference 6.

3. Numerical and Experimental Results

To validate the present analysis, various numerical examples are considered. As a simple case, open-ended waveguide structures excited by a dominant mode field and radiating into half space through an infinite ground plane are analyzed. To study the effect of a finite ground plane, this paper considers a coaxially fed cavity that excites a coaxial aperture in a finite ground plane. The numerical data for these cases are compared with earlier published results and the experimental data obtained at NASA Langley Research Center.

3.1. Apertures in Infinite Ground Plane

3.1.1. Rectangular aperture. A rectangular aperture as shown in figure 2(a) with dimensions $a = 4.755$ cm, $b = 2.215$ cm, and $L = 1.9$ cm in an infinite ground plane and excited by a rectangular waveguide loaded with a dielectric plug ($\varepsilon_r = 3.76$) is considered. The dielectric plug is discretized using 1230 tetrahedral elements. The air-dielectric interface inside the waveguide is considered as the input plane. The dominant TE_{10} mode is considered to be incident at the plane $z = -L$. The input admittance of this structure is calculated as a function of frequency and plotted in figure 2(b). The numerical results agree very well with the data presented by Swift (ref. 16).

3.1.2. Circular aperture. A circular aperture in an infinite ground plane and excited by a circular waveguide is considered as a second example. The geometry is shown in figure 3(a). The circular waveguide of length $L = \lambda$ from the aperture is considered as a circular cavity for FEM discretization. The waveguide is discretized at a level of 0.1λ. The dominant TE_{11} mode is considered to be incident at the plane $z = -L$. The input admittance is computed as a function of the radius of the waveguide and plotted in figure 3(b) along with the numerical data given by Bailey and Swift (ref. 17). The results computed using the present technique and those of reference 17 agree very well.

3.1.3. Coaxial aperture. As a third example, a coaxial aperture excited by a coaxial line is considered. The geometry is shown in figure 4(a). Again the coaxial line of length $L = \lambda$ from the aperture is considered as a coaxial cavity for FEM discretization. The coaxial line is discretized at a level of 0.1λ. Only the dominant TEM mode is considered for both incident and reflected fields in the coaxial feed line because the higher order modes do not seem to contribute to the final result. (See appendix section A.3.) The input admittance is computed as a function of frequency and plotted in figure 4(b). The results are compared with the available data in the literature (ref. 18).

3.2. Apertures in Finite Ground Plane

To verify the validity of the current method when combined with GTD, a coaxial cavity with a finite ground plane is considered. The geometry of the cavity is shown in figure 5. The cavity is fed by a coaxial line with the center conductor extending up to the radiating aperture. The cavity volume is discretized using 4474 tetrahedral elements, resulting in 4904 unknowns. For experimental verification, the cavity with dimensions as given in figure 5 was fabricated and its input-return loss and radiation patterns as a function of frequency measured. Figure 6 presents the input-return loss computed using the present method, assuming infinite ground plane, along with the experimental results. The finite ground plane in this case does not affect the input-return loss properties.

The far-field patterns for the structure shown in figure 5 were calculated with equation (37) for two frequencies, 5.0 GHz and 9.0 GHz. Figures 7 and 8 show the calculated values along with the experimental data. The good agreement between the calculated results and the experimental data validates the present analysis. Because the radiation pattern of an antenna depends upon the aperture field, it is useful to know the tangential electric field at the aperture of the structure (shown in fig. 5). In figures 9 and 10 the tangential electric field at the aperture is plotted for 5.0 GHz and 9.0 GHz, respectively. As expected, the aperture field deviates from the TEM field distribution as the frequency increases.

4. Conclusions

A combined finite element method/method of moments/geometrical theory of diffraction (FEM/MoM/GTD) technique was presented to analyze radiation from cavity-backed apertures with finite ground planes. Various numerical examples were considered to demonstrate the flexibility and validity of the method. The numerical data obtained using the present method and the data available in the literature agree very well. The successful application of the GTD was demonstrated by calculating the radiation patterns of a coaxial cavity with finite ground plane and comparing the theoretical results with the experimental data. By virtue of the FEM, this combined FEM/MoM/GTD technique is applicable to arbitrarily shaped cavities filled with inhomogeneous and anisotropic materials. With proper modeling, microstrip antenna arrays residing in cavities with finite ground planes can be also analyzed. This technique can also be easily extended to a finite circular ground plane.

NASA Langley Research Center
Hampton, VA 23681-0001
September 6, 1995

Appendix

Modal Expansions of Feed Structures

For completeness, expressions for the modal expansions of electric fields (eq. (19)) at the input plane of feed structures are given below, with the incident field given by equation (20).

A.1 Rectangular Waveguide

The cross section of the input plane of the rectangular waveguide is shown in figure A1. The incident electric field is assumed to be the dominant TE_{10} mode, which is given by

$$\left.\begin{aligned} \mathbf{e}_{\text{inc}} &= -y\sqrt{\frac{2}{ab}}\cos\left(\frac{\pi x}{a}\right) \\ \gamma_{\text{inc}} &= j\sqrt{k_o^2-\left(\frac{\pi}{a}\right)^2} \end{aligned}\right\} \tag{A1}$$

The reflected electric fields for TE and TM modes are written with mode $m = (p, q)$ as (ref. 10)

$$\begin{aligned} \mathbf{e}_m^{TE} &= A_{pq}\mathbf{x}\left(\frac{q\pi}{b}\right)\cos\left[\frac{p\pi}{a}\left(x+\frac{a}{2}\right)\right]\sin\left[\frac{q\pi}{b}\left(y+\frac{b}{2}\right)\right] \\ &\quad - A_{pq}\mathbf{y}\left(\frac{p\pi}{a}\right)\sin\left[\frac{p\pi}{a}\left(x+\frac{a}{2}\right)\right]\cos\left[\frac{q\pi}{b}\left(y+\frac{b}{2}\right)\right] \end{aligned}$$

(p and q = 0, 1, 2, …; if $p = 0$, $q \neq 0$; if $q = 0$, $p \neq 0$) (A2)

and

$$\begin{aligned} \mathbf{e}_m^{TM} &= \mathbf{x}A_{pq}\left(\frac{p\pi}{a}\right)\cos\left[\frac{p\pi}{a}\left(x+\frac{a}{2}\right)\right]\sin\left[\frac{q\pi}{b}\left(y+\frac{b}{2}\right)\right] \\ &\quad + \mathbf{y}A_{pq}\left(\frac{q\pi}{b}\right)\sin\left[\frac{p\pi}{a}\left(x+\frac{a}{2}\right)\right]\cos\left[\frac{q\pi}{b}\left(y+\frac{b}{2}\right)\right] \\ &\quad + \mathbf{z}\frac{A_{pq}}{\gamma_m}\left[\left(\frac{p\pi}{a}\right)^2+\left(\frac{q\pi}{b}\right)^2\right]\sin\left[\frac{p\pi}{a}\left(x+\frac{a}{2}\right)\right]\cos\left[\frac{q\pi}{b}\left(y+\frac{b}{2}\right)\right] \end{aligned}$$

(p = 0, 1, 2, 3, …; q = 0, 1, 2, 3, …) (A3)

where

$$A_{pq} = \sqrt{\frac{\varepsilon_{op}\varepsilon_{oq}}{ab}}\,\frac{1}{\sqrt{\left(\frac{p\pi}{a}\right)^2+\left(\frac{q\pi}{b}\right)^2}} \tag{A4}$$

$$\varepsilon_{op} = \begin{cases} 2 & (\text{for } p \neq 0) \\ 1 & (\text{for } p = 0) \end{cases}$$

and

$$\varepsilon_{oq} = \begin{cases} 2 & (\text{for } q \neq 0) \\ 1 & (\text{for } q = 0) \end{cases}$$

$$\gamma_m = \begin{cases} j\sqrt{k_o^2 - \left(\frac{p\pi}{a}\right)^2 + \left(\frac{q\pi}{b}\right)^2} & k_o^2 \geq \left(\frac{p\pi}{a}\right)^2 + \left(\frac{q\pi}{b}\right)^2 \\ \sqrt{\left(\frac{p\pi}{a}\right)^2 + \left(\frac{q\pi}{b}\right)^2 - k_o^2} & k_o^2 < \left(\frac{p\pi}{a}\right)^2 + \left(\frac{q\pi}{b}\right)^2 \end{cases} \quad \text{(A5)}$$

A.2 Circular Waveguide

The cross section of the input plane of the circular waveguide is shown in figure A2. The incident electric field is assumed to be the dominant TE_{11} mode, which is given by

$$\mathbf{e}_{\text{inc}} = A_{11}\left\{\hat{\rho}\left[-\frac{1}{\rho}J_1(k'_\rho\ \rho)\cos\phi\right] + \hat{\phi}[k'_\rho\ J'_1\ (k'_\rho\ \rho)\sin\phi]\right\} \quad \text{(A6)}$$

and

$$\gamma_{\text{inc}} = j\sqrt{k_o^2 - k'^2_\rho} \quad \text{(A7)}$$

where $k'_\rho = \frac{\chi'_{11}}{r_c}$ and χ'_{11} represents the first zero of the derivative of the Bessel function J_1. Equation (A9) defines A_{11} with $p = 1$ and $q = 1$. The reflected electric fields for TE and TM modes with $m = (p, q)$ are given by

$$\mathbf{e}_m^{TE} = A_{pq}\left\{\hat{\rho}\left[-\frac{q}{\rho}J_q(k'_\rho\ \rho)\cos(q\phi)\right] + \hat{\phi}[k'_\rho\ J'_q\ (k'_\rho\ \rho)\sin(q\phi)]\right\} \quad \text{(A8)}$$

$$\mathbf{e}_m^{TM} = B_{pq}\left\{\hat{\rho}[k_\rho J'_q\ (k_\rho\rho)\sin(q\phi)] + \hat{\phi}\left[\frac{q}{p}J_q(k_\rho\rho)\cos(q\phi)\right]\right\}$$
$$+ \mathbf{z}\frac{B_{pq}}{\gamma_m}[(k_o^2 + \gamma_m^2)J_q(k_\rho\rho)\sin(q\phi)] \quad \text{(A9)}$$

where $k'_\rho = \frac{\chi'_{pq}}{r_c}$ and $k_\rho = \frac{\chi_{pq}}{r_c} \cdot \chi'_{pq}$ is the pth zero (p = 1, 2, …) of the derivative of the Bessel function J_q of the first kind of order q (q = 0, 1, 2, …). χ_{pq} is the pth zero (p = 1, 2, 3, …) of the Bessel function J_q of the first kind of order q (q = 0, 1, 2, …), and

$$A_{pq} = \sqrt{\frac{\varepsilon_{oq}}{\pi(\chi'^2_{pq} - q^2)}}\ \frac{1}{J_q(\chi'_{pq})} \quad \text{(A10)}$$

$$B_{pq} = \sqrt{\frac{\varepsilon_{oq}}{\pi}}\ \frac{1}{\chi_{pq}J'_q(\chi_{pq})} \quad \text{(A11)}$$

$$\gamma_m = \left\{ \begin{array}{ll} j\sqrt{k_o^2 - \kappa^2} & (k_o > \kappa) \\ \sqrt{\kappa^2 - k_o^2} & (k_o \le \kappa) \end{array} \right\} \tag{A12}$$

where $\kappa = k'_\rho$ for TE modes and $\kappa = k_\rho$ for TM modes.

A.3 Coaxial Line

The cross section of the input plane of the coaxial line is shown in figure A3. The incident electric field is assumed to be the dominant TEM mode and is given by

$$\mathbf{e}_{\text{inc}} = \hat{\rho} \frac{1}{\sqrt{2\pi \ln\left(\frac{r_2}{r_1}\right)}} \frac{1}{\rho} \tag{A13}$$

$$\gamma_{\text{inc}} = jk_o \tag{A14}$$

In a practical feed-line arrangement, the coaxial line is relatively small in diameter and the amplitudes of the higher order coaxial modes that are excited are small. A reasonable approximation is to assume that only a reflected TEM mode exists in the coaxial line. Hence, in equation (19),

$$\mathbf{e}_m^{TE} = \hat{\rho} \frac{1}{\sqrt{2\pi \ln\left(\frac{r_2}{r_1}\right)}} \frac{1}{\rho} \tag{A15}$$

$$\mathbf{e}_m^{TM} = 0 \tag{A16}$$

$$\gamma_m = jk_o \tag{A17}$$

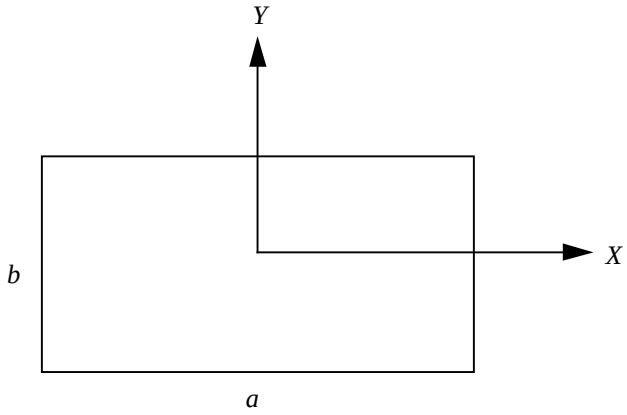

Figure A1. Cross section of rectangular waveguide.

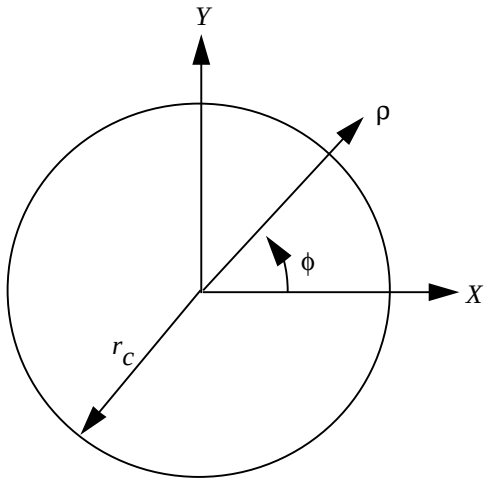

Figure A2. Cross section of circular waveguide.

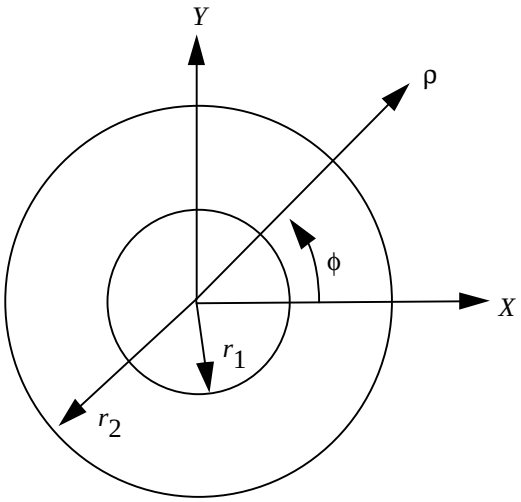

Figure A3. Cross section of coaxial line.

References

1. Jin, J. M.; and Volakis, J. L.: A Hybrid Finite Element Method for Scattering and Radiation by Microstrip Patch Antennas and Arrays Residing in a Cavity. *IEEE Trans. Antennas & Propag.*, vol. 39, no. 11, Nov. 1991, pp. 1598–1604.

2. Chatterjee, A.; Jin, J. M.; and Volakis, J. L.: Edge-Based Finite Elements and Vector ABC's Applied to 3-D Scattering. *IEEE Trans. Antennas & Propag.*, vol. 41, no. 2, Feb. 1993, pp. 221–226.

3. Jin, J. M.; and Volakis, J. L.: A Finite Element-Boundary Integral Formulation for Scattering by Three-Dimensional Cavity-Backed Apertures. *IEEE Trans. Antennas & Propag.*, vol. 39, no. 1, Jan. 1991, pp. 97–104.

4. Yuan, X.: Three-Dimensional Electromagnetic Scattering From Inhomogeneous Objects by the Hybrid Moment and Finite Element Method. *IEEE Trans. Microw. Theory & Tech.*, vol. 38, issue 8, Aug. 1990, pp. 1053–1058.

5. Jin, Jian-Ming: *The Finite Element Method in Electromagnetics*, John Wiley & Sons, 1993.

6. Cockrell, C. R.; and Pathak, P. H.: Diffraction Theory Techniques Applied to Aperture Antennas on Finite Circular and Square Ground Planes. *IEEE Trans. Antennas & Propag.*, vol. AP-22, May 1974, pp. 443–448.

7. Sun, W.; and Balanis, C. A.: Edge-Based FEM Solution of Scattering From Inhomogeneous and Anisotropic Objects. *IEEE Trans. Antennas & Propag.*, vol., 42, issue 5, May 1994, pp. 627–632.

8. Silvester, P. P.; and Ferrari, R. L.: *Finite Elements for Electrical Engineers*, Second ed., Cambridge Univ. Press, 1990.

9. Reddy, C. J.; Deshpande, Manohar D.; Cockrell, C. R.; and Beck, Fred B.: *Finite Element Method for Eigenvalue Problems in Electromagnetics.* NASA TP-3485, 1994.

10. Harrington, Roger F.: *Time-Harmonic Electromagnetic Fields.* McGraw-Hill Book Co., Inc. 1961.

11. Rao, S. M.; Glisson, A. W.; and Wilton, D. R.: Electromagnetic Scattering by Surfaces of Arbitrary Shape. *IEEE Trans. Antennas & Propag.*, vol. AP-30, May 1982, pp. 409–418.

12. Zienkiewicz, O. C.: *The Finite Element Method in Engineering Science.* McGraw-Hill Book Co., Inc., 1971.

13. Wilton, Donald R.; Rao, S. M.; Glisson, Allen W.; Schaubert, Daniel H.; Al-Bundak, O. M.; and Butler, Chalmers M.: Potential Integrals for Uniform and Linear Source Distributions on Polygonal and Polyhedral Domains. *IEEE Trans. Antennas & Propag*., vol. AP-32, no. 3, Mar. 1984, pp. 276–281.

14. Sarkar, Tapan K.; Yang, Xiaopu; and Arvas, Ercument: Limited Survey of Various Conjugate Gradient Methods for Solving Complex Matrix Equations Arising in Electromagnetic Wave Interactions. *Wave Motion*, vol. 10, no. 6, Dec. 1988, pp. 527–546.

15. Pathak, P. H.; and Kouyoumjian, R. G.: *The Dyadic Diffraction Coefficient for a Perfectly Conducting Wedge.* AFCRL-69-0546, U.S. Air Force, 1969. (Available from DTIC as AD 707 827.)

16. Swift, Calvin T.: Admittance of a Waveguide-Fed Aperture Loaded With a Dielectric Plug. *IEEE Trans. Antennas & Propag.*, vol. AP-17, no. 3, May 1969, pp. 356–359.

17. Bailey, Marion C.; and Swift, Calvin T.: Input Admittance of a Circular Waveguide Aperture Covered by a Dielectric Slab. *IEEE Trans. Antennas & Propag.*, vol. AP-16, no. 4, July 1968, pp. 386–391.

18. Swift, Calvin T.: *Input Admittance of a Coaxial Transmission Line Opening Onto a Flat, Dielectric Covered Ground Plane*. NASA TN D-4158, 1967.

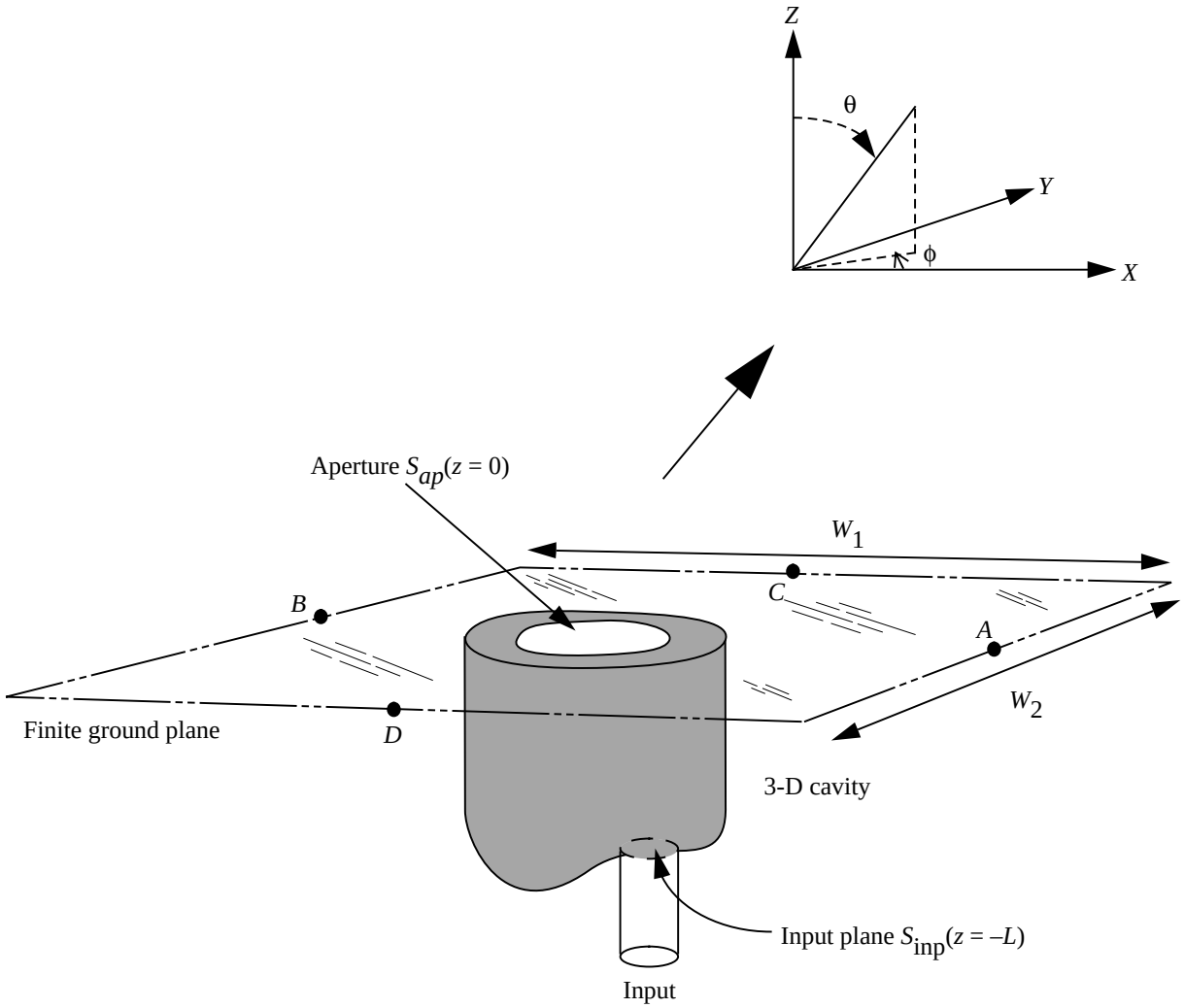

Figure 1. Geometry of cavity-backed aperture in finite ground plane.

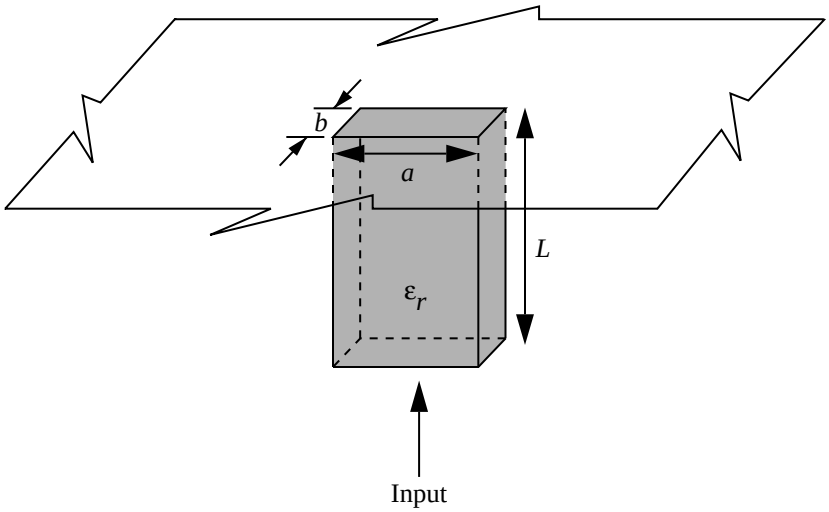

(a) Rectangular waveguide with dielectric plug radiating into half space.

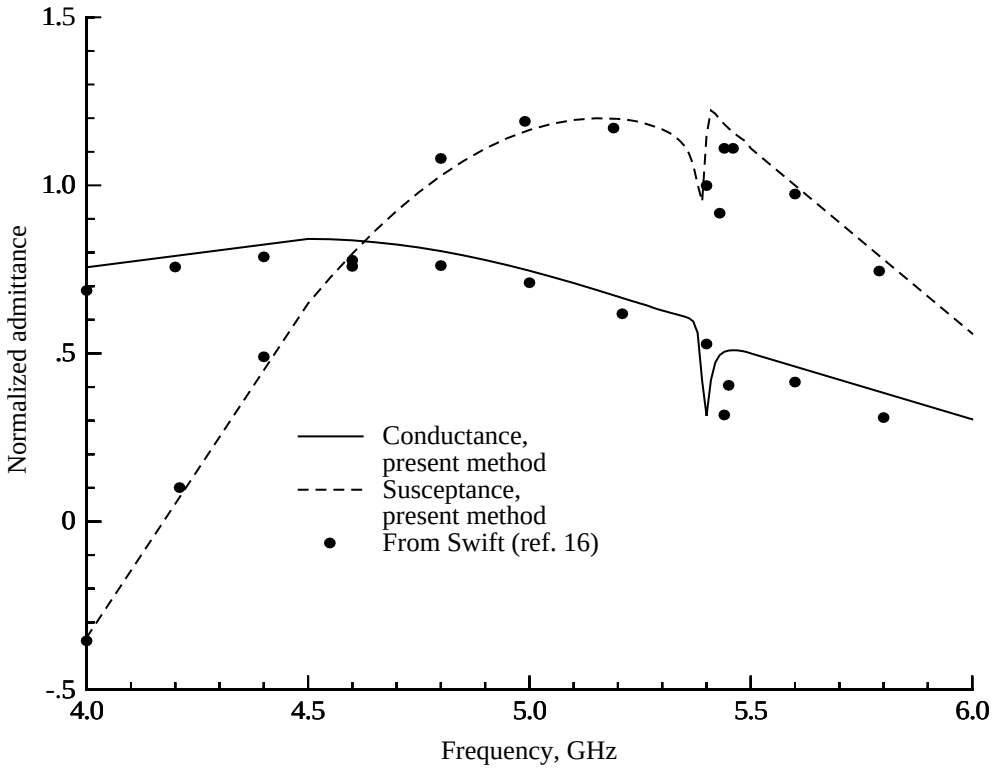

(b) Variation of normalized admittance with frequency for case a = 4.755 cm, b = 2.215 cm, L = 1.9 cm, and ε_r = 3.76.

Figure 2. Rectangular aperture in infinite ground plane.

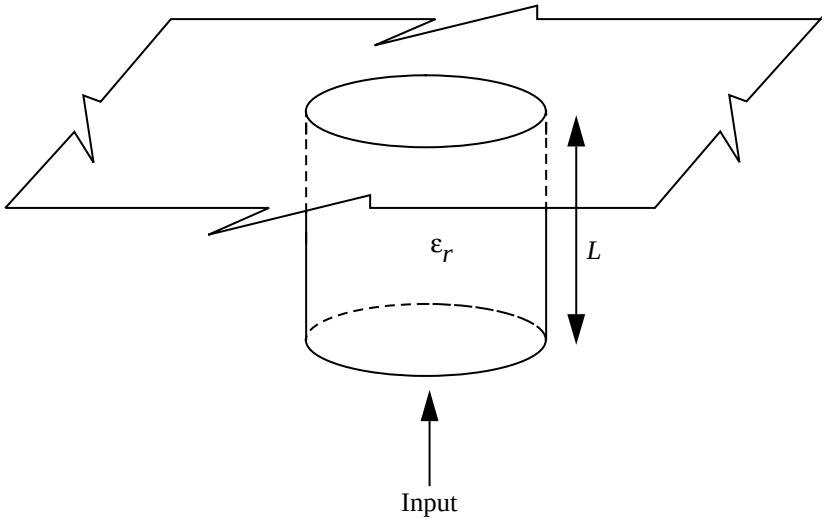

(a) Circular waveguide with radius r radiating into half space.

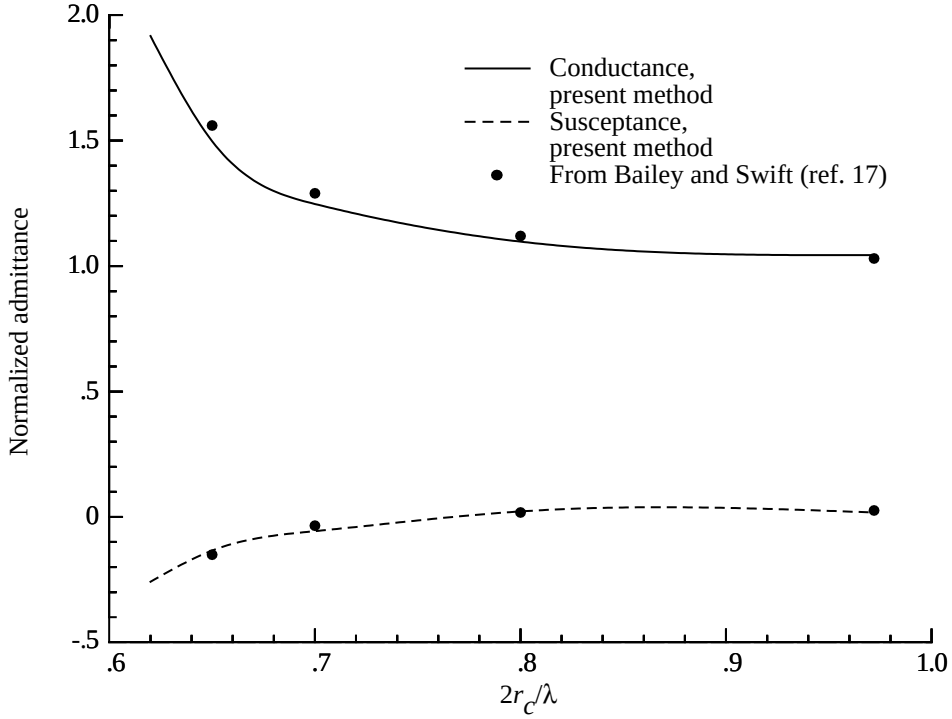

(b) Input admittance as function of $2r_c/\lambda$ for case $L = \lambda$ and $\varepsilon_r = 1.0$.

Figure 3. Circular aperture in infinite ground plane.

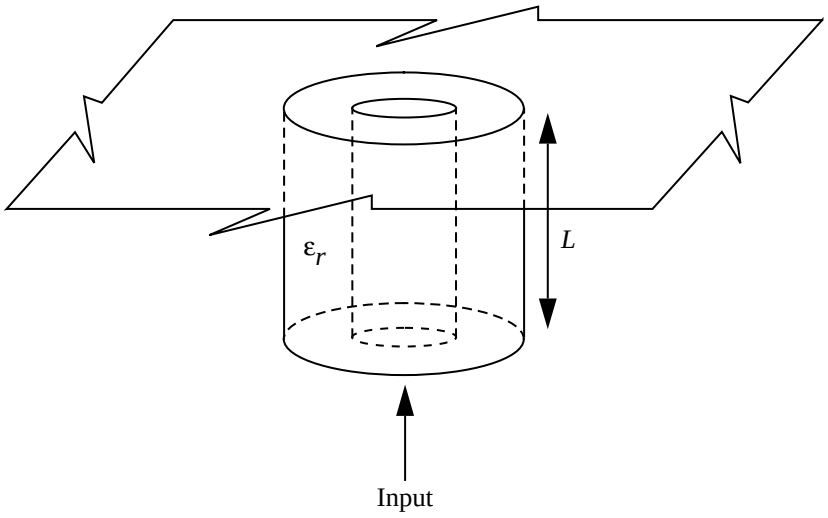

(a) Coaxial line with inner radius r_1 and outer radius r_2 radiating into half space.

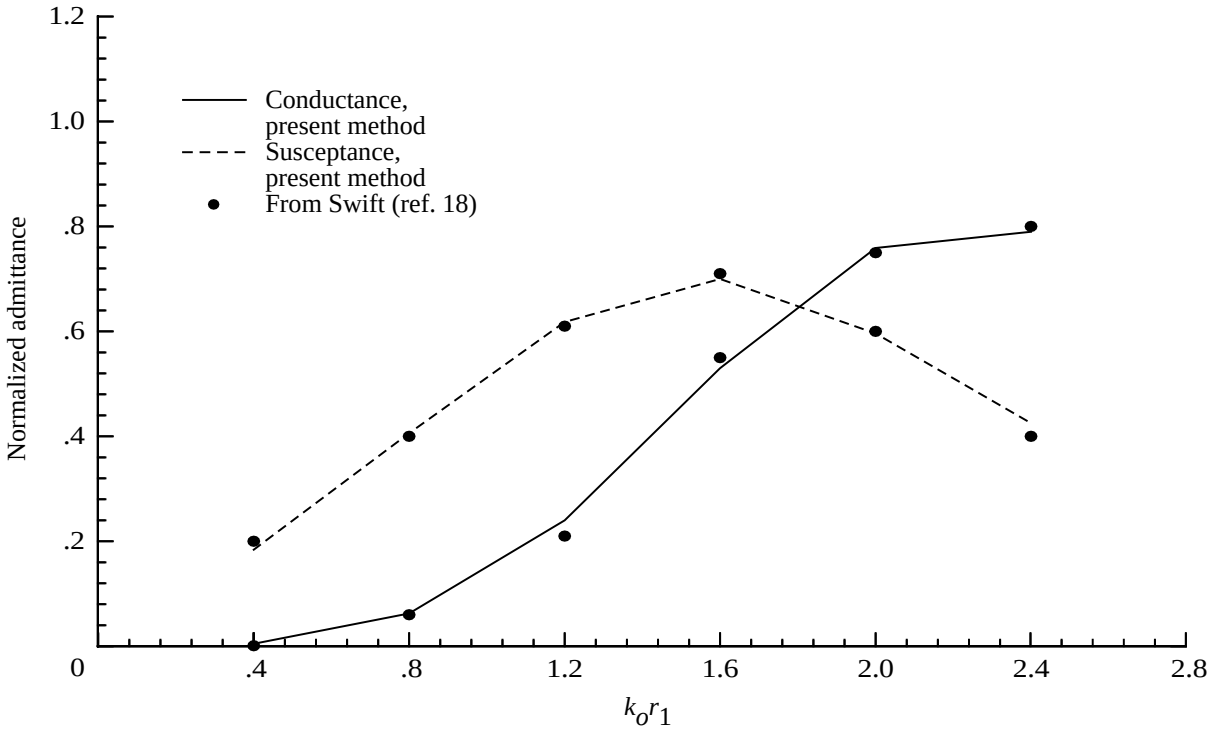

(b) Input admittance as function of $k_o r_1$ for case $r_2/r_1 = 1.57$, $L = \lambda$, and $\varepsilon_r = 1.0$.

Figure 4. Coaxial aperture excited by coaxial line.

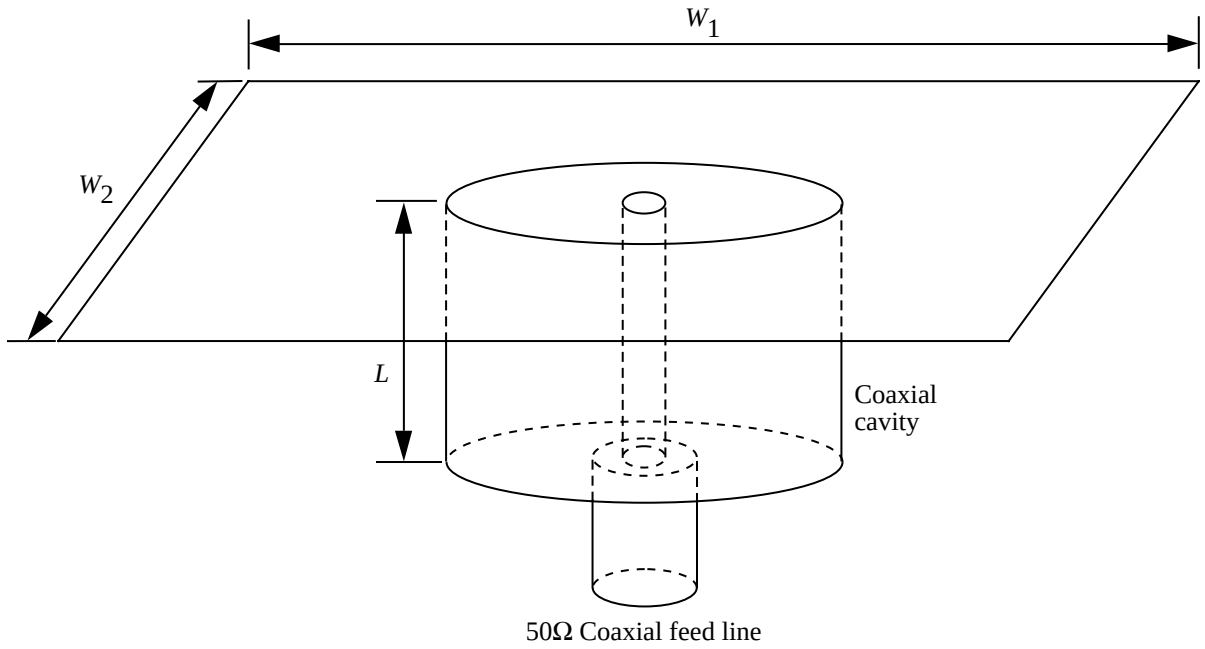

Figure 5. Geometry of coaxial cavity with finite rectangular ground plane. W_1 = 24 in.; W_2 = 12 in.; L = 3/8 in.; Outer radius of coaxial cavity = 1 in.; Inner radius of coaxial cavity = 0.0181 in.; cavity fed by 50Ω coaxial line.

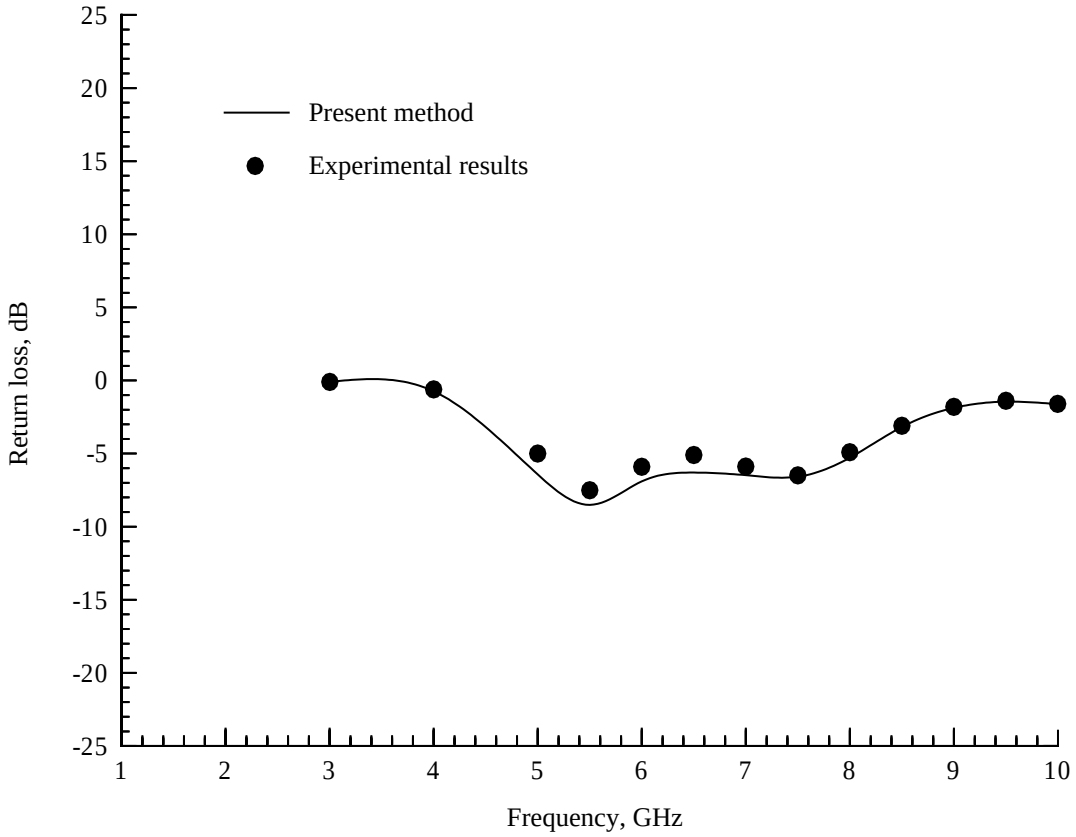

Figure 6. Return loss of coaxial cavity (fig. 5) with frequency.

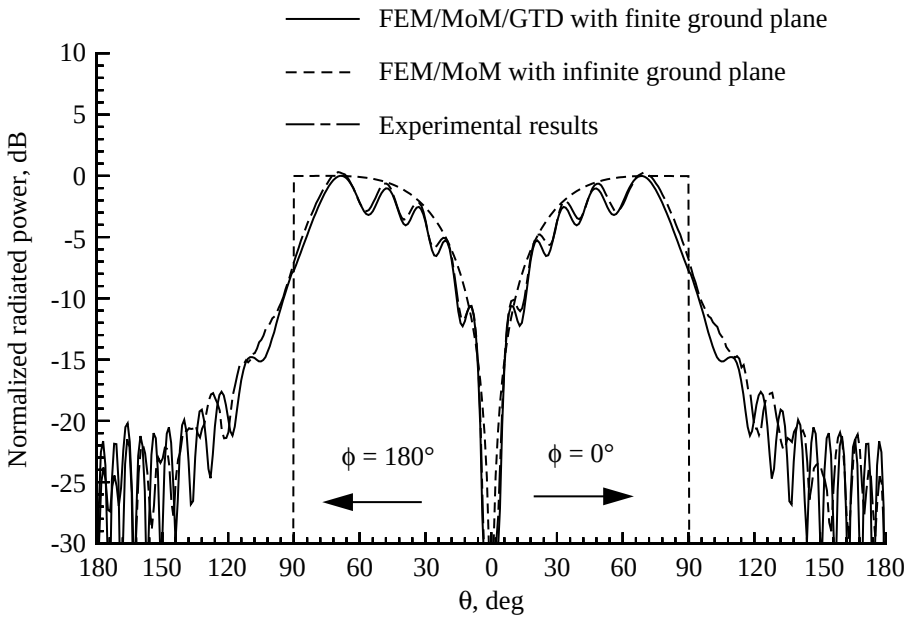

(a) Radiation pattern of coaxial cavity at $\phi = 0°$ and $\phi = 180°$.

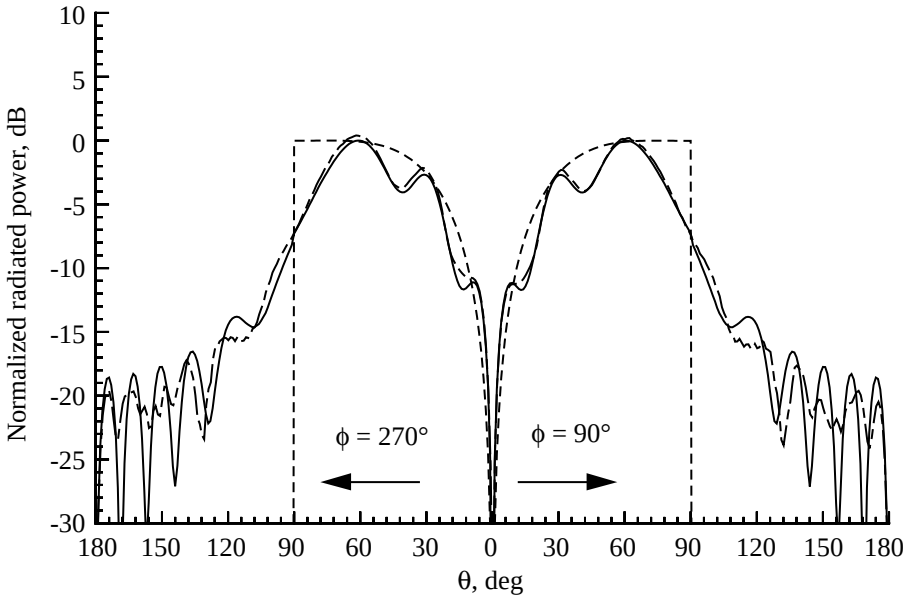

(b) Radiation pattern of coaxial cavity at $\phi = 90°$ and $\phi = 270°$.

Figure 7. Far-field patterns at 5.0 GHz.

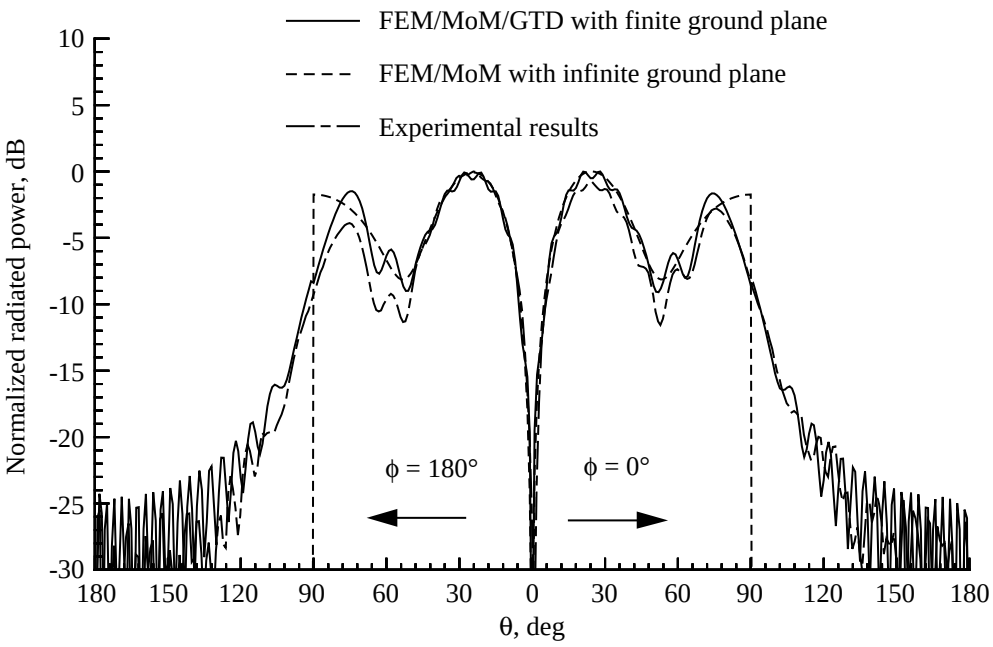

(a) Radiation pattern of coaxial cavity at $\phi = 0°$ and $\phi = 180°$.

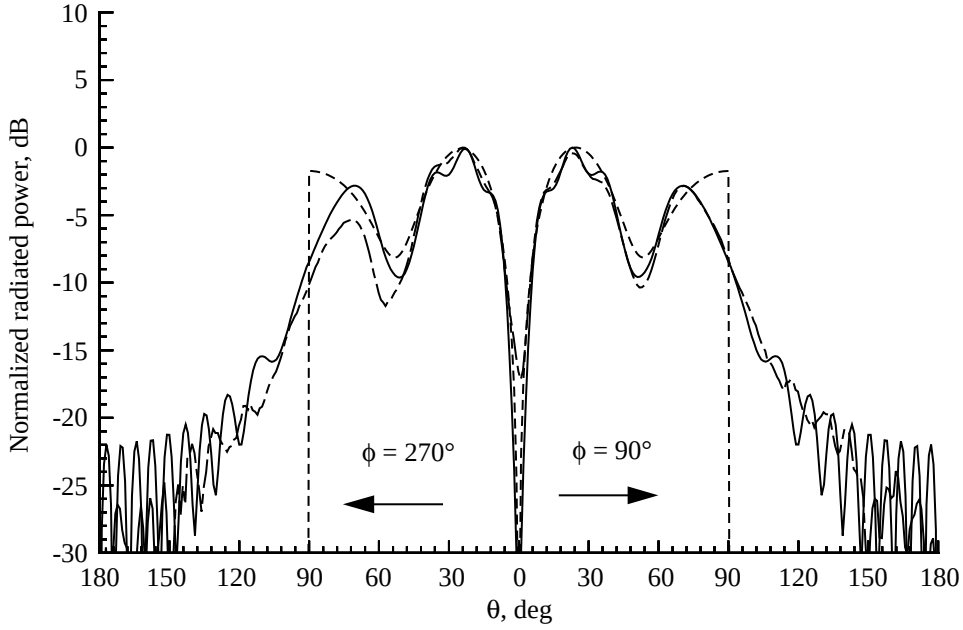

(b) Radiation pattern of coaxial cavity at $\phi = 90°$ and $\phi = 270°$.

Figure 8. Far-field patterns at 9.0 GHz.

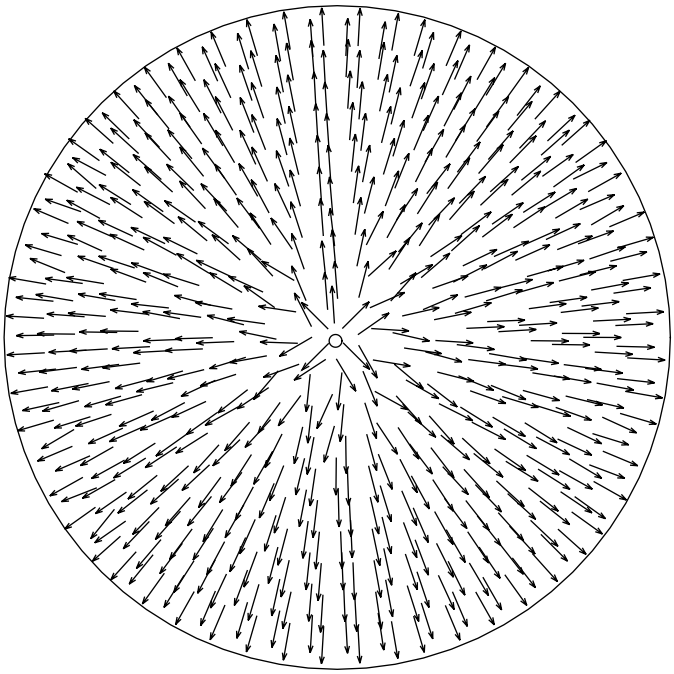

Figure 9. Vector plot of electric field at coaxial-cavity aperture at 5.0 GHz. Amplitudes have been equalized for clarity of presentation.

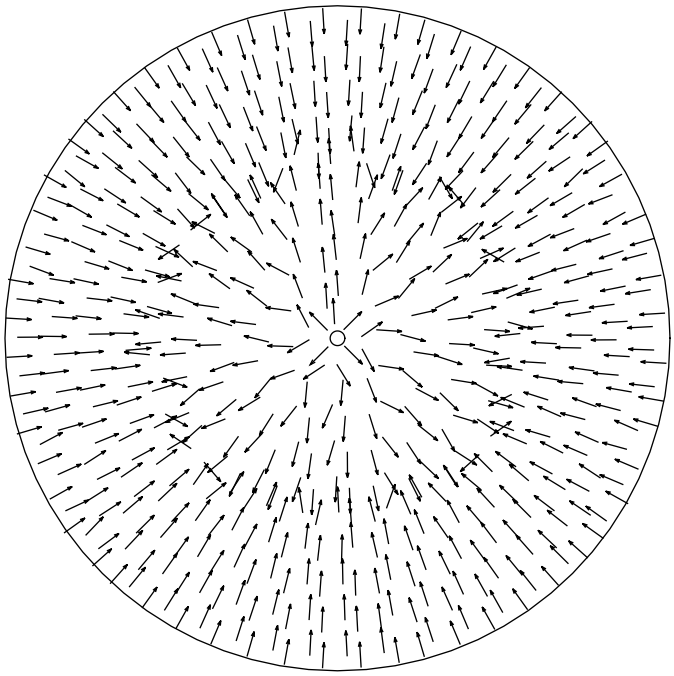

Figure 10. Vector plot of electric field at coaxial-cavity aperture at 9.0 GHz. Amplitudes have been equalized for clarity of presentation.

REPORT DOCUMENTATION PAGE

Form Approved
OMB No. 0704-0188

1. AGENCY USE ONLY *(Leave blank)*	2. REPORT DATE	3. REPORT TYPE AND DATES COVERED
	November 1995	Technical Paper

4. TITLE AND SUBTITLE
Analysis of Three-Dimensional-Cavity-Backed Aperture Antennas Using a Combined Finite Element Method/Method of Moments/Geometrical Theory of Diffraction Technique

5. FUNDING NUMBERS
WU 505-64-70-01

6. AUTHOR(S)
C. J. Reddy, M. D. Deshpande, C. R. Cockrell, and F. B. Beck

7. PERFORMING ORGANIZATION NAME(S) AND ADDRESS(ES)
NASA Langley Research Center
Hampton, VA 23681-0001

8. PERFORMING ORGANIZATION REPORT NUMBER
L-17482

9. SPONSORING/MONITORING AGENCY NAME(S) AND ADDRESS(ES)
National Aeronautics and Space Administration
Washington, DC 20546-0001

10. SPONSORING/MONITORING AGENCY REPORT NUMBER
NASA TP-3548

11. SUPPLEMENTARY NOTES
Reddy: NRC-NASA Resident Research Associate, Langley Research Center, Hampton, VA; Deshpande: ViGYAN, Inc., Hampton, VA; Cockrell and Beck: Langley Research Center, Hampton, VA.

12a. DISTRIBUTION/AVAILABILITY STATEMENT
Unclassified–Unlimited
Subject Category 17
Availability: NASA CASI (301) 621-0390

12b. DISTRIBUTION CODE

13. ABSTRACT *(Maximum 200 words)*
A combined finite element method (FEM) and method of moments (MoM) technique is presented to analyze the radiation characteristics of a cavity-fed aperture in three dimensions. Generalized feed modeling has been done using the modal expansion of fields in the feed structure. Numerical results for some feeding structures such as a rectangular waveguide, circular waveguide, and coaxial line are presented. The method also uses the geometrical theory of diffraction (GTD) to predict the effect of a finite ground plane on radiation characteristics. Input admittance calculations for open radiating structures such as a rectangular waveguide, a circular waveguide, and a coaxial line are presented. Numerical data for a coaxial-fed cavity with finite ground plane are verified with experimental data.

14. SUBJECT TERMS
Antennas; Cavity backed; Finite element method; Method of moments; Geometrical theory of diffraction

15. NUMBER OF PAGES
26

16. PRICE CODE
A03

17. SECURITY CLASSIFICATION OF REPORT	18. SECURITY CLASSIFICATION OF THIS PAGE	19. SECURITY CLASSIFICATION OF ABSTRACT	20. LIMITATION OF ABSTRACT
Unclassified	Unclassified	Unclassified	